Nuclear Materials and Energy 45 (2025) 102031

Contents lists available at ScienceDirect

Nuclear Materials and Energy

journal homepage: www.elsevier.com/locate/nme

Modelling of tungsten prompt redeposition at the inner wall of ITER during ramp-up☆

A. Kirschner [a,*], C. Baumann [a], S. Brezinsek [a], Ch. Linsmeier [a], R.A. Pitts [b], A.A. Pshenov [b], J. Romazanov [a]

[a] Forschungszentrum Jülich GmbH, Institute of Fusion Energy and Nuclear Waste Management – Plasma Physics, 52425 Jülich, Germany
[b] ITER Organization, Route de Vinon-sur-Verdon, CS 90 046, 13067 St Paul Lez Durance Cedex, France

ARTICLE INFO

Keywords:
Plasma-wall interaction
Prompt redeposition
Erosion
Tungsten
ERO code
ITER

ABSTRACT

The prompt redeposition of sputtered tungsten at the inner wall of ITER during current ramp-up has been simulated with the ERO code. Plasma parameters from SOLPS-ITER for a medium-density (with a peak electron density of 4E12 cm^{-3} at the inner wall) and a high-density (1E13 cm^{-3}) case have been used as input for ERO. Simulations without anomalous cross-field diffusion for sputtered tungsten ions reveal peaked prompt redeposition profiles in poloidal direction. At the tangency point with largest electron temperature and density, maximum prompt redeposition fractions of about 60 % for the medium density and 80 % for the high density case occur. At a distance of 50 cm away from the tangency point, prompt redeposition decreases to 10 % (medium-density) and 20 % (high-density case). The simulations without anomalous cross-field diffusion show that the overall redeposition is the same as the prompt redeposition thus the overall redeposition is only due to prompt redeposition. An anomalous cross-field diffusion of 1 m^2/s leads to slightly increased prompt redeposition, however, for both medium and high-density case there is now also a significant amount of non-prompt redeposition. The modelled profiles of prompt redeposition can be used as input for plasma simulation codes like SOLPS-ITER to improve the assumptions of net tungsten wall sources.

1. Introduction

In the past, intense research has been undertaken to study carbon-based materials as first wall element in fusion devices. As low-Z element the tolerable concentration of carbon in the core plasma is comparably high and the non-existence of melting has been seen as great advantage since problems due to melting do not exist. However, in addition to physical sputtering the disadvantage of chemical erosion – a process which also is present at the lowest plasma temperatures – has been identified as major drawback. The fusion community came to the conclusion, that carbon-based materials are unsuitable as first wall material in fusion power plants in particular due to long-term tritium retention in co-deposited layers as consequence of chemical erosion, as well as net erosion thickness incompatible with high duty operation of a reactor and dust production. Substantial work on carbon chemical erosion and its influence on tritium retention has been provided by Joachim Roth, here just a few of his game-changing publications are mentioned [1–4]. Also based on Roth`s work, see for example the estimation of long-term tritium retention in ITER with different wall material mixes in [4], the decision has been taken to exclude carbon as divertor material and beryllium as main wall material from ITER and instead to construct a full-tungsten device [5]. The general trend of these predictions was confirmed in the JET tokamak with transition from a full carbon device to a beryllium main wall and tungsten divertor configuration [6]. In addition it should be mentioned that besides tritium retention equally important for the abandoning of beryllium as main wall material in ITER were licensing requirements and dust production issues.

Tungsten as high-Z material has a relatively low physical sputtering. Chemical erosion – if occurring at all – is negligibly small [7]. In addition, tungsten has a very large melting point of about 3400 °C. However, the core plasma tungsten concentration in a fusion device has to be kept at extremely low values around 3E-5 to minimize plasma dilution and in particular plasma cooling [8]. Therefore, it is of great importance to

☆ This article is part of a special issue entitled: 'PWI – J. Roth' published in Nuclear Materials and Energy.

* Corresponding author.
E-mail address: a.kirschner@fz-juelich.de (A. Kirschner).

https://doi.org/10.1016/j.nme.2025.102031
Received 15 October 2025; Received in revised form 11 November 2025; Accepted 17 November 2025
Available online 19 November 2025

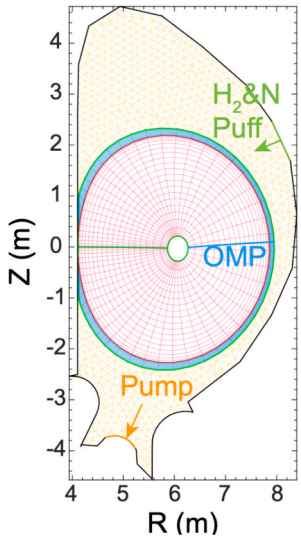

Fig. 1. Simulation grid used for the SOLPS-ITER simulations of ITER limiter configuration during current ramp-up [18].

control and minimize the net source of tungsten from the various wall elements. In this context prompt redeposition, which primarily happens for high-Z elements of large mass like tungsten, is an important process, which significantly can reduce the gross erosion to much smaller net erosion. The term "prompt redeposition" has first been introduced by Fussmann et al. [9] as redeposition of sputtered particles before finishing their first gyration orbit. A simplified analytical formula has been derived to estimate the fraction of singly ionised particles promptly redeposited. That formula only depends on the ratio of ionisation length and gyration radius of sputtered particles and in particular does not consider the effect of the electric sheath field. Afterwards, Naujoks et al. have used the 3D Monte-Carlo code ERO to refine the estimations of tungsten prompt redeposition [10] taking into account the sheath electric field and also e.g. multiple ionisation of the sputtered tungsten particles. In the meanwhile, further theoretical work on prompt redeposition has been published, as example Particle-In-Cell simulations [11], detailed studies with the ERO code [12] or semi-empirical estimations [13] are referred. One main conclusion of all these approaches is that the electric field is an important contributor for prompt redeposition. Also, experimental approaches have been done, either based on in-situ spectroscopic observations, see e.g. [14–16] or on post-mortem analysis, e.g. [17]. In particular, the spectroscopic approach typically only can provide a lower limit of prompt redeposition, however, the experimental observations are in line with corresponding modelled results. Furthermore, thorough early studies of tungsten retention and resulting central tungsten concentration in a full tungsten device have been performed in ASDEX Upgrade, see for instance [18] and references therein.

The present work provides the modelling of poloidal tungsten prompt redeposition profiles at the inner wall of ITER during ramp-up. During ramp-up the plasma has a limiter configuration with direct contact to the inner wall potentially leading to large tungsten source. Therefore, the amount of tungsten prompt redeposition is of particular importance as it reduces the net tungsten source. The estimated prompt redeposition fraction can be used in plasma simulation codes to improve the assumption of net tungsten source as typically prompt redeposition is not considered at all or set to an arbitrary value in such plasma simulations. First results of prompt redeposition for ITER ramp-up cases have been published in [19], however, the present work covers a wider range of parameters and provides additional results not discussed in [19].

2. Modelling of tungsten prompt redeposition

2.1. Assumptions for the modelling

To simulate the prompt tungsten redeposition the 3D Monte-Carlo code ERO [10,20,21] is used. ERO calculates the transport of sputtered particles within the edge plasma considering all important

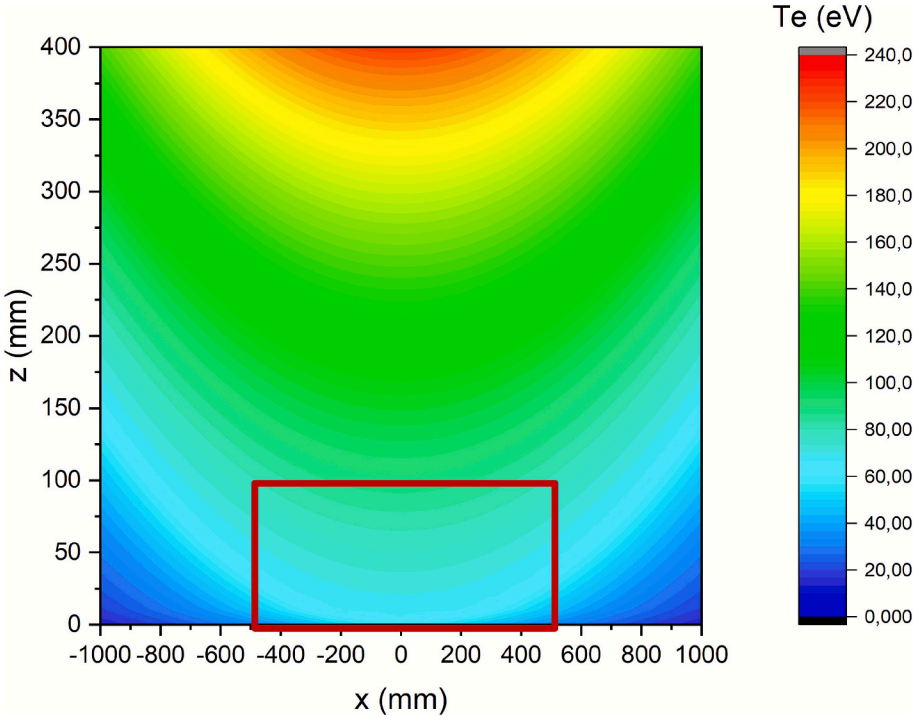

Fig. 2. Electron temperature T_e for the high-density case from SOLPS-ITER. The red rectangular indicates the ERO simulation volume. The coordinate "x" refers to the ITER coordinate "Z", the coordinate "z" corresponds to the radial direction of ITER.

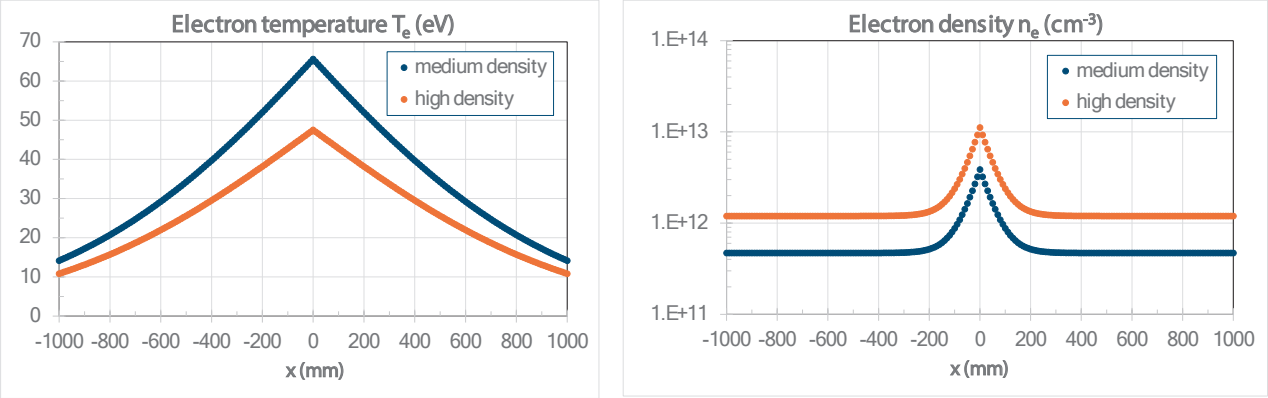

Fig. 3. Profiles of the electron temperature T_e and density n_e along the inner wall for the medium and high-density case.

processes like gyration, electric sheath, multiple ionisation, friction force, thermal force, anomalous cross-field diffusion, and reflection. Sputtered tungsten particles start from the surface as neutrals with a cosine angular distribution and a Thompson energy distribution. Ionisation and recombination of tungsten particles is calculated by means of the ADAS database [22]. Within the present work sputtered particles, which are deposited within a time smaller or equal than their gyration time, are defined as promptly redeposited.

The necessary background plasma parameters for the ERO calculations are provided by SOLPS-ITER simulations for two different cases of limiter configuration during ramping [19]: a medium and a high density $<n_{e,LCFS}>$ case. The according configuration is shown in Fig. 1 demonstrating the ramp-up with the plasma contacting the inner wall of ITER. The ERO simulations cover a small volume from $-0.5\ m \leq Z \leq +0.5\ m$ and extending 0.1 m in radial direction R. For the current study the small size of the simulation volume is sufficient as the focus lies on prompt redeposition calculations around the tangency point Z = 0 mm where the plasma touches the wall and largest gross erosion is expected. Also, as prompt redeposition is a very localised process, particle losses at the edges of the small simulation volume will not significantly change the main results. Fig. 2 shows as example the 2D distribution of the electron density for the high-density case with the ERO-coordinates "x" (corresponding to the ITER coordinate "Z") and "z" (corresponding to the ITER coordinate "R"). In toroidal direction the plasma is assumed to be constant. Fig. 3 presents the profiles of electron temperature T_e and density n_e along the inner wall for the medium and high-density case. The profiles are very peaked with the maximum at the midplane, x = 0 mm. The peak values of electron density and temperature for the medium-density case are about 4E12 cm^{-3} and 65 eV, for the high-density case about 1E13 cm^{-3} and 50 eV.

2.2. Modelling results

The modelled distribution of tungsten atoms W^0 and ions W^+ and W^{2+} is shown in Fig. 4 exemplarily for the high-density case. For comparison simulations without anomalous cross-field diffusion for tungsten ions and with $D_{perp} = 1\ m^2/s$ are presented. As expected, the penetration of sputtered tungsten is smallest around the midplane x = 0 mm as there the plasma parameters have their maximum. At the edges x= ± 500 mm of the simulation volume the penetration depth is about 50 mm demonstrating that there is no significant loss of particles in radial direction whereas particles not redeposited leave the simulation volume mainly in toroidal direction. The distribution with cross-field diffusion results in ion trajectories which are more aligned along the z-axis. Also, the tungsten ions penetrate deeper into the plasma compared to the simulation without cross-field diffusion, this is in particular obvious around x = 0 mm. It has to be noted that the gross tungsten erosion flux Γ_{gross} is calculated in a simplified manner assuming a constant B field angle at the surface of $\alpha_B = 1°$ along the wall and applying $\Gamma_{gross} = c_s \cdot n_e \cdot \sin(\alpha_B) \cdot Y_{D\text{-}W}$ with c_s the sound speed and $Y_{D\text{-}W}$ the physical sputtering yield of tungsten due to deuterium. In reality, the magnetic field angle varies along the surface and at the present shallow magnetic field cross-field transport effects have to be considered to estimate the impacting background fluxes. Moreover, under the present plasma conditions, tungsten sputtering will be dominated by impurities (oxygen, seed species) and also energetic CX neutrals should be considered [23,24]. However, the current work focuses on the fraction of prompt redeposition, which is independent of the original gross erosion source. The absolute magnitude of the erosion flux is not part of the present studies.

The resulting profiles of overall and prompt redeposition relative to the gross erosion are summarised in Fig. 5a) for the medium and Fig. 5b) for high-density case. As can be seen, the overall redeposition fraction can be larger than 100 % as particles, which are not promptly redeposited (i.e. not in the vicinity of the location of erosion), can be redeposited at other locations where then the overall redeposition (prompt plus non-prompt) can become larger than 100 % relative to the gross erosion at that location. Without cross-field diffusion all tungsten redeposition is by means of prompt redeposition. As expected from the plasma parameter profiles, the redeposition is peaked around the midplane position x = 0 mm. The maximum prompt redeposition fraction at the peak is about 60 % for the medium and about 80 % for the high-density case. At the edges of the simulation volume x = ± 500 mm the amount of prompt redeposition decreases to ~10 % for the medium and ~20 % for the high-density case. With $D_{perp} = 1\ m^2/s$, also non-prompt redeposition occurs with profiles less peaked compared to prompt redeposition. The overall redeposition fraction reaches values up to 100 % at x = 0 mm for both medium and high-density case. The prompt redeposition fraction slightly increases with perpendicular diffusion, at the peak up to ~70 % for the medium and ~90 % for the high-density case is reached.

The profiles of the mean charge <Q> of all redeposited particles is summarised in Fig. 6a). For both medium and high-density case, the mean charge without cross-field diffusion peaks at x = 0 mm with <Q> ~1.5 and decreases to <Q> ~1.0 farther away. Considering cross-field diffusion results in <Q> ~ 2 around x = 0 mm and somewhat increased <Q> ~2.5 farther away, again with no significant difference between medium and high-density case. The higher charge states in the simulations with considering perpendicular diffusion result from deeper penetration of the tungsten particles to higher plasma density and temperature regions, see Fig. 4. The profiles of mean charge for promptly redeposited tungsten ions (Fig. 6b)) resemble the ones from

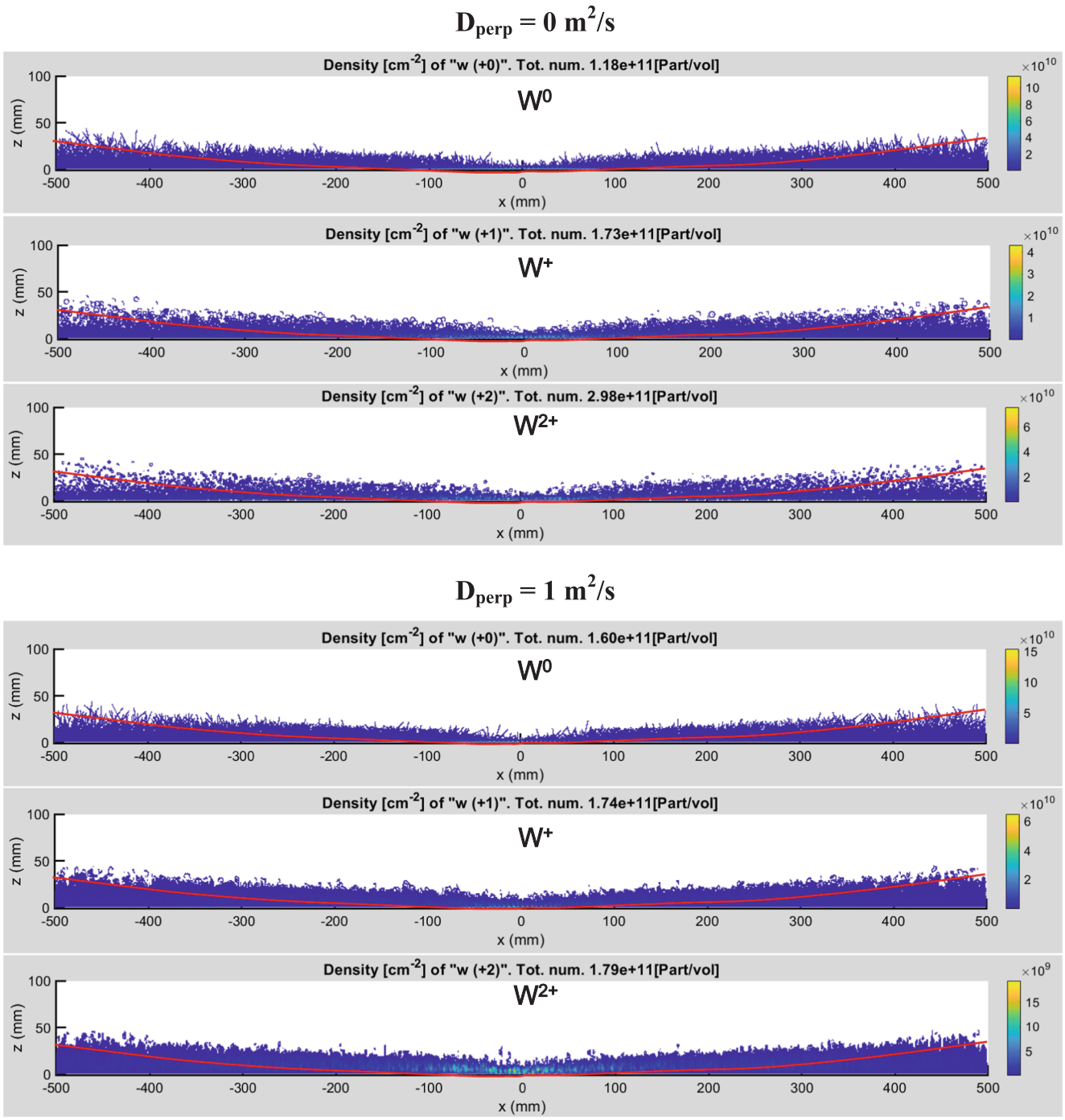

Fig. 4. Distribution of sputtered tungsten atoms W^0 and resulting W^+ and W^{2+} ions simulated for the high-density case. The red curves indicate the last closed flux surface LCFS.

Fig. 6a) for the case without cross-field diffusion – this is expected as without cross-field diffusion redeposition is only due to prompt redeposition.

Finally, Fig. 7 presents the amount of tungsten self-sputtering (relative to the gross erosion by the background plasma) caused by locally returning tungsten ions at different ionisation stages – tungsten particles from global migration pathways are not included here. The modelled profiles are similar for the medium and high-density case but show significantly larger self-sputtering for the cases with anomalous cross-field diffusion, which can be explained by the higher charge states of returning tungsten ions with cross-field diffusion, see Fig. 6a), and thus, larger impact energy according to $3 \cdot \langle Q \rangle \cdot T_e$, with $3 \cdot T_e$ the sheath potential. The maximum amount of self-sputtering occurs at x = 0 mm due to maximum plasma temperature at this location and varies between 20 % (no cross-field diffusion) and 40 % (with $D_{perp} = 1\ m^2/s$). Also, for the cases without cross-field-diffusion, the shapes of the self-sputtering profiles resemble the profiles of prompt redeposition (Fig. 5) with a peak around x = 0 mm. The self-sputtering profiles for the cases with cross-field diffusion are much broader and thus similar to the profiles of the overall redeposition.

3. Conclusions

Profiles of prompt tungsten redeposition have been modelled with

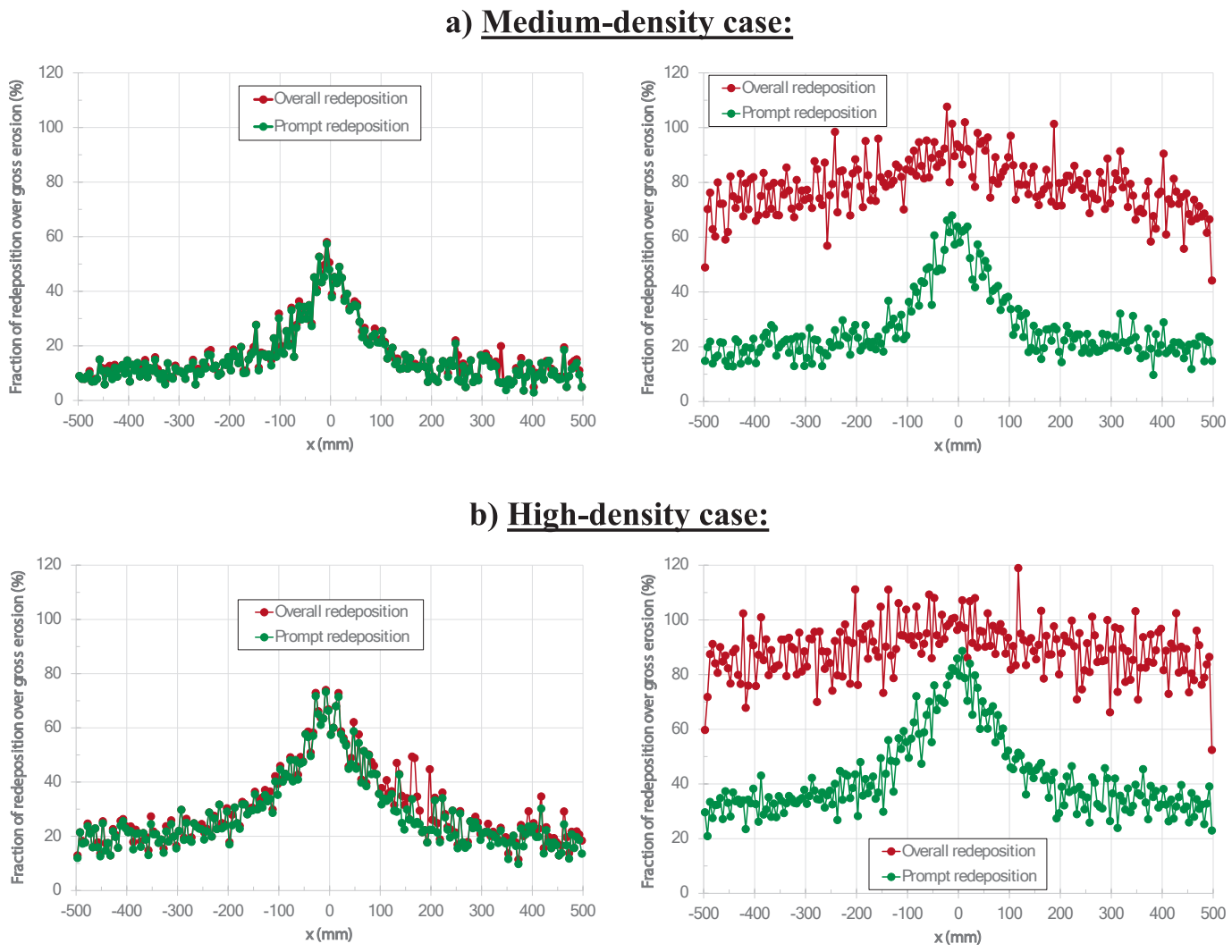

Fig. 5. Profiles of overall and prompt tungsten redeposition along the inner wall without and with cross-field diffusion for tungsten ions. **a)** Medium-density case and **b)** High-density case.

the ERO code for ITER current ramp-up phases at the inner wall. SOLPS-ITER simulations of the according limiter plasmas have been used as input for ERO focussing on a medium and a high-density case. The amount of prompt redeposition poloidally varies with maximum values at the midplane position. For the cases studied, the prompt redeposition fraction at the maximum varies between 60 % and 90 %. Larger prompt redeposition occurs for the high-density case and for the simulations with consideration of an anomalous cross-field diffusion for tungsten ions. The modelled tungsten redeposition fractions are in line with spectroscopic analysis at TEXTOR resulting in a lower limit of tungsten redeposition of about 50 % at plasma conditions very similar to the peak values of the high-density case [14].

Whereas typically prompt redeposition is neglected in plasma simulation codes, the present results can be incorporated in such simulations and significantly help to better describe the net tungsten source which finally is important with respect to plasma contamination.

The local ERO simulations provide robust results of prompt redeposition fractions and are suitable for parameter studies due to reasonable computational times. Though, to investigate the destiny of particles lost from the small simulation volume, more costly global simulations have to be done, e.g. with ERO2.0, which is a task for the future.

CRediT authorship contribution statement

A. Kirschner: Writing – original draft, Visualization, Software, Methodology, Investigation, Conceptualization. **C. Baumann:** Writing – review & editing, Data curation. **S. Brezinsek:** Writing – review & editing, Supervision, Funding acquisition, Formal analysis, Conceptualization. **Ch. Linsmeier:** Writing – review & editing, Conceptualization. **R.A. Pitts:** Writing – review & editing, Conceptualization. **A.A. Pshenov:** Writing – review & editing, Conceptualization. **J. Romazanov:** Writing – review & editing, Conceptualization.

Declaration of competing interest

The authors declare that they have no known competing financial interests or personal relationships that could have appeared to influence the work reported in this paper.

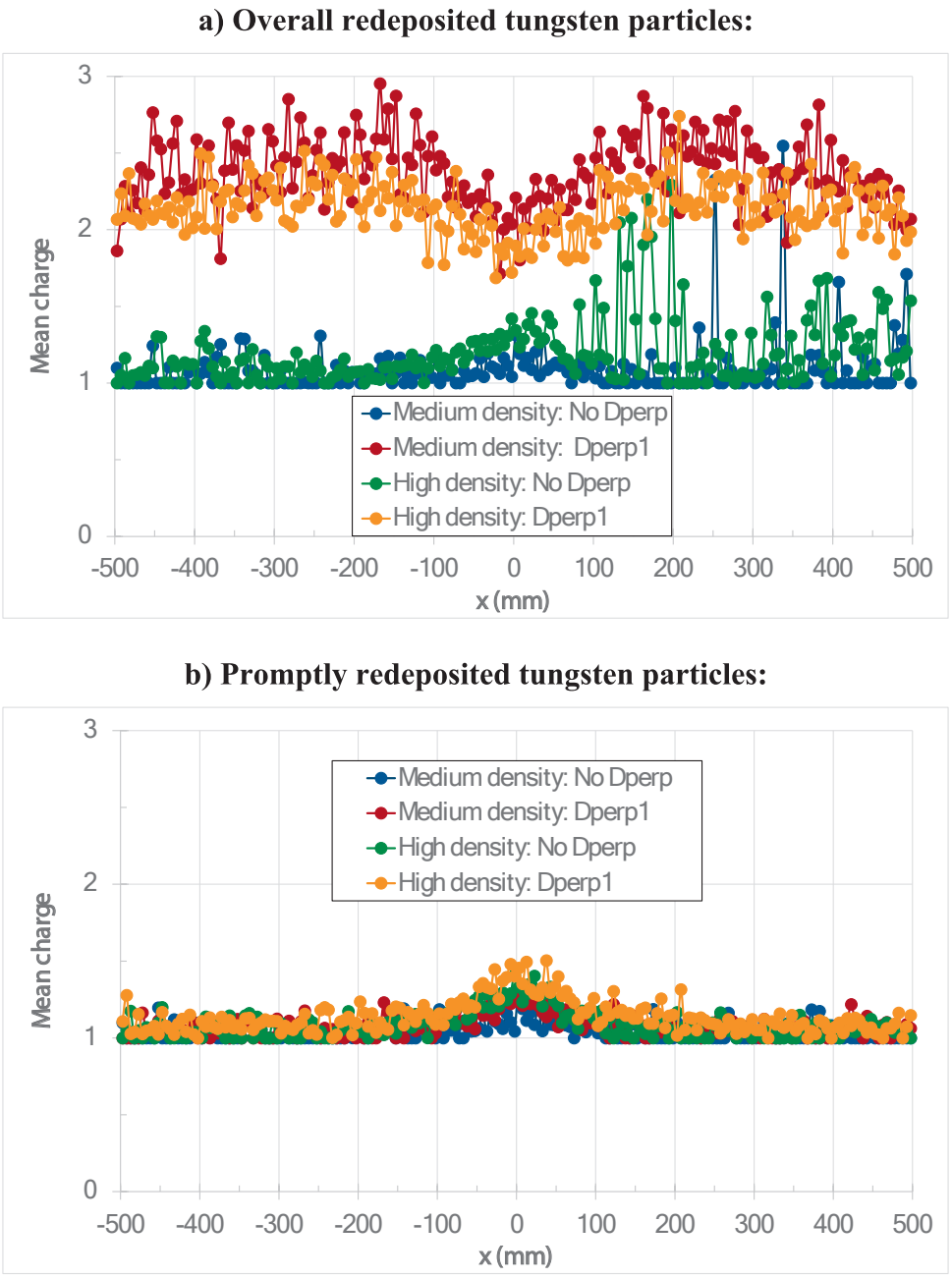

Fig. 6. **a)** Mean charge of all redeposited tungsten particles. **b)** Mean charge of promptly redeposited ones. Simulations without anomalous cross-field diffusion (**No Dperp**) are compared with the ones including anomalous cross-field diffusion of $D_{perp} = 1$ m^2/s for tungsten ions (**Dperp1**).

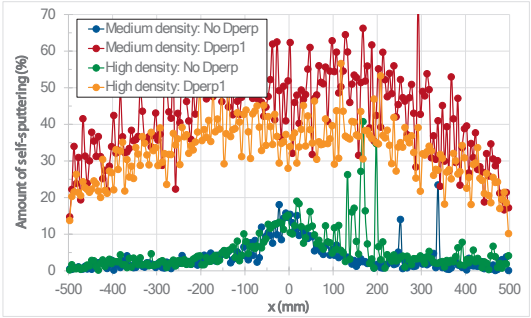

Fig. 7. Amount of tungsten self-sputtering caused by locally returning tungsten ions. Simulations without anomalous cross-field diffusion (**No Dperp**) are compared with the ones including anomalous cross-field diffusion of $D_{perp} = 1$ m^2/s for tungsten ions (**Dperp1**).

Acknowledgement

This work has been carried out within the framework of the EUROfusion Consortium, funded by the European Union via the Euratom Research and Training Programme (Grant Agreement No 101052200 — EUROfusion). Views and opinions expressed are however those of the author(s) only and do not necessarily reflect those of the European Union or the European Commission. Neither the European Union nor the European Commission can be held responsible for them.

Data availability

Data will be made available on request.

References

[1] J. Roth, Phys. Scr. T124 (2006) 37.
[2] J. Roth, R. Preuss, W. Bohmeyer, S. Brezinsek, et al., Nucl. Fusion 44 (2004) L21.
[3] J. Roth, A. Kirschner, R. Preuss, W. Bohmeyer, et al., J. Nucl. Mater. 337 (2005) 970.
[4] J. Roth, E. Tsitrone, A. Loarte, Th. Loarer, et al., J. Nucl. Mater. 390 (2009) 1.
[5] R.A. Pitts, A. Loarte, T. Wauters, M. Dubrov, et al., Nucl. Mater. Energy 42 (2025) 101854.
[6] S. Brezinsek, T. Loarer, V. Philipps, H.G. Esser, et al., Nucl. Fusion 53 (2013) 083023.
[7] S. Brezinsek, A. Pospieszczyk, G. Sergienko, R. Dux, et al., Nucl. Mater. Energy 18 (2019) 50.
[8] T. Pütterich, R. Neu, R. Dux, A.D. Whiteford, et al., Nucl. Fusion 50 (2010) 025012.
[9] G. Fussmann, W. Engelhardt, D. Naujoks, K. Asmussen, et al., Plasma Phys. Controlled Nucl. Fusion Res. 2 (1994) 143.
[10] D. Naujoks, K. Asmussen, M. Bessenrodt-Weberpals, S. Deschka, et al., Nucl. Fusion 36 (1996) 671.
[11] D. Tskhakaya, M. Groth, JET EFDA contributors, J. Nucl. Mater. 463 (2015) 624.
[12] A. Kirschner, D. Tskhakaya, S. Brezinsek, D. Borodin, et al., Plasma Phys. Controlled Fusion 60 (2018) 014041.
[13] L. Cappelli, N. Fedorczak, E. Serre, Nucl. Fusion 64 (2024) 106028.
[14] S. Brezinsek, D. Borodin, J.W. Coenen, D. Kondratjew, et al., Phys. Scr. T145 (2011) 014016.
[15] G.J. van Rooij, J.W. Coenen, L. Aho-Mantila, S. Brezinsek, et al., J. Nucl. Mater. 438 (2013) S42.
[16] T. Abrams, J.G. Guterl, S. Abe, D.C. Donovan, et al., Mater. Res. Express (2023) 126503.
[17] D.L. Rudakov, P.C. Stangeby, W.R. Wampler, J.N. Brooks, et al., Phys. Scr. T159 (2014) 014030.
[18] R. Neu, A. Kallenbach, M. Balden, V. Bobkov, et al., J. Nucl. Mater. 438 (2013) S34.
[19] Y. Zhang, A.A. Pshenov, R.A. Pitts, X. Bonnin, et al., Nucl. Fusion 65 (2025) 056035.
[20] D. Naujoks, R. Behrisch, J.P. Coad, L.C.J.M. de Kock, Nucl. Fusion 33 (1993) 581.
[21] A. Kirschner, V. Philipps, J. Winter, U. Kögler, Nucl. Fusion 50 (2000) 989.
[22] H.P. Summers, The ADAS User Manual, version 2.6 (http://adas.ac.uk).
[23] H.A. Kumpulainen, M. Groth, S. Brezinsek, F. Casson, et al., Plasma Phys. Controlled Fusion 66 (2024) 055007.
[24] C. Baumann, J. Romazanov, D. Matveev, A. Kirschner, et al, submitted to Nuclear Fusion.